11 Superconductivity and Magnetism

M. Bendele, S. Bosma (since November 2009), Z. Guguchia (since September 2009), A. Ichsanov (since October 2009), H. Keller, F. Murányi, P. Prem, J. Roos, S. Strässle, S. Weyeneth, B. M. Wojek

Visiting scientists: M. V. Eremin, B. Graneli, B. I. Kochelaev, R. Puzniak, A. Shengelaya
Emeritus members: K. A. Müller (Honorarprofessor), T. Schneider (Titularprofessor), M. Mali

in collaboration with:
ETH Zürich (J. Karpinski), Paul Scherrer Institute (K. Conder, R. Khasanov, E. Morenzoni), Max-Planck-Institute for Solid State Research Stuttgart (A. Bussmann-Holder), IBM Rüschlikon Research Laboratory (J. G. Bednorz, S. F. Alvarado), University of Geneva (Ø. Fischer, J. M. Triscone), University of Rome (D. Di Castro), Kazan State University (A. Dooglav, M. V. Eremin, B. I. Kochelaev), Polish Academy of Sciences (R. Puzniak), Tbilisi State University (A. Shengelaya), University of Tokyo (T. Sasagawa, H. Takagi), University of British Columbia (R. F. Kiefl).

In the following we report on selected projects in the research field of high-temperature superconductors (HTS) and materials with novel electronic properties. Our recent activities include studies by means of a variety of techniques, such as of muon-spin rotation (μSR), electron paramagnetic resonance (EPR), nuclear magnetic resonance (NMR), nuclear quadrupole resonance (NQR), and SQUID and torque magnetometry. Besides focusing on the cuprates and other, more conventional superconductors, the investigations have been further extended to the recently discovered iron-based superconductors.

11.1 Field dependent superfluid density in optimally doped $SmFeAsO_{1-x}F_y$

After the discovery of superconductivity in $LaFeAsO_{1-x}F_x$ with a transition temperature $T_c \simeq 26$ K, a whole new family of iron pnictide superconductors was found (1) with a maximum $T_c \simeq 55$ K for $SmFeAsO_{1-x}F_y$ (2). Various experiments indicate multi-gap superconductivity within the family $RE FeAsO_{1-x}F_y$ (RE = rare-earth element) (3). Furthermore, the magnetic penetration depth anisotropy, $\gamma_\lambda = \lambda_c/\lambda_{ab}$, increases with decreasing temperature, in contrast to the upper critical field anisotropy, $\gamma_H = H_{c2}^{||ab}/H_{c2}^{||c}$, which decreases with decreasing temperature (3; 4), similar to that of the two-gap superconductor MgB_2 (5; 6), although with reversed slopes. Here λ_i and $H_{c2}^{||i}$ denote the magnetic penetration depth and the upper critical field components, respectively, along the crystallographic direction i (ab-plane or c-axis).

Besides of the influence of the magnetic field H and temperature T on the anisotropy, the direct influence of H and T on λ is essential in probing multi-gap superconductivity (7). Importantly, the superfluid density $\rho_s = n_s/m^*$, with n_s being the superfluid carrier density and m^* the effective carrier mass, can be probed directly by measuring $\lambda^{-2} \propto \rho_s$.

A single crystal sample of nominal composition $SmFeAsO_{0.8}F_{0.2}$ was investigated by torque magnetometry in order to determine $\lambda_{ab}(H)$. The magnetic torque $\vec{\tau} = \mu_0(\vec{m} \times \vec{H})$, related to the magnetic moment $\vec{m}$, was recorded in dependence of the angle θ between the magnetic field $\vec{H}$ and the c-axis of the crystal. During the measurement, H was rotated clockwise and counterclockwise around the sample at constant temperature T. The clockwise (θ^+) and counterclockwise

(θ^-) torque scans were averaged according to $\tau_{\rm rev}(\theta) = [\tau(\theta^+) + \tau(\theta^-)]/2$. A theoretical expression for the angular dependence of the torque, involving the two anisotropy parameters γ_λ and γ_H independently (8), was used to analyze the data. Representative experimental torque data collected for various magnetic fields together with the calculated curves are presented in Fig. 11.1. Obviously λ_{ab} increases substantially with increasing magnetic field (see insert to Fig. 11.1) (8).

In accordance with the result in Fig. 11.1, the data plotted in terms of the superfluid density λ_{ab}^{-2} imply a suppression of the superfluid density as the field is increased. The field dependence of λ_{ab}^{-2}, derived from the torque experiment together with μSR data taken on a larger powder sample of the same compound, are presented in Fig. 11.2. Evidently, λ_{ab}^{-2} gets substantially suppressed with increasing magnetic field at all temperatures studied and falls, when normalized to $\lambda_{ab}^{-2}(1.4\,{\rm T}/\mu_0)$, on a universal curve (see Fig. 11.2). We estimate a suppression of the superfluid density by 20% as the field increases from 0 to 1.4 T (8).

The observed magnetic field dependence of λ_{ab}^{-2} is absent in single-gap superconductors but has been observed in various multi-band superconductors, where the cases of MgB_2 (7; 9) and $La_{1.83}Sr_{0.17}CuO_4$ (10) have been analyzed in detail. The analogy to these systems suggests that related physics applies here. Assuming that $SmFeAsO_{1-x}F_y$ is a fully-gapped superconductor, a two-gap model (8; 11) is used to calculate the superfluid density $\rho_{\rm s} = \rho_{\rm s1} + \rho_{\rm s2}$, stemming from the two coupled gaps (Δ_1, Δ_2). Within this approach the calculated zero-temperature gaps are $\Delta_1(0) = 13.83$ meV and $\Delta_2(0) = 5.26$ meV. With increasing magnetic field the superfluid density is only suppressed in the band with the small gap $(\rho_{\rm s2}, \Delta_2)$ where the corresponding intra-band interaction approaches zero with increasing field. The total superfluid density $\rho_{\rm s}(H)$ is expressed as a sum of a contribution from the band with the large gap, $\rho_{\rm s1}$, which

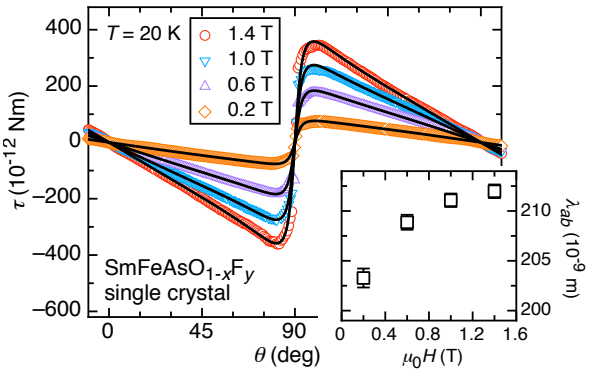

Figure 11.1: Angular dependent, reversible torque for single crystal $SmFeAsO_{1-x}F_y$ in various magnetic fields. Solid lines are fits to the data, from which λ_{ab} was extracted. The insert shows the field dependence of λ_{ab}.

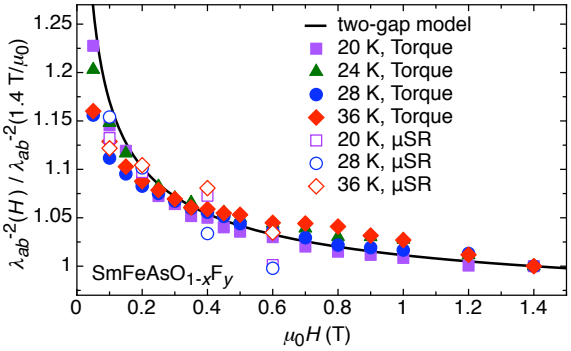

Figure 11.2: Universal behavior of $\rho_{\rm s}$ of single crystal $SmFeAsO_{1-x}F_y$ observed for all investigated temperatures, determined by magnetic torque and μSR experiments, normalized to 1.4 T. The black line is calculated using a two-gap model.

is independent of the field, and a field dependent contribution from the band with the small gap, $\rho_{\rm s2} \propto 1/\sqrt{H}$. A fit to the normalized superfluid density data (see Fig. 11.2) gives good agreement. It is important to emphasize that although $\rho_{\rm s}$ is suppressed by 20% in small fields, $T_{\rm c}$ is almost not changing on the same field scale, consistent with high values of $H_{\rm c2}$. This can be understood in terms of a suppression of the intra-band coupling within the band of the small gap, having a pronounced influence on the corresponding $\rho_{\rm s}$, but almost no effect on $T_{\rm c}$ (9).

[1] Y. Kamihara *et al.*, J. Am. Chem. Soc. **130**, 3296 (2008).
[2] Z.-A. Ren *et al.*, Chin. Phys. Lett. **25**, 2215 (2008).
[3] S. Weyeneth *et al.*, J. Supercond. Nov. Magn. **22**, 347 (2009).
[4] S. Weyeneth *et al.*, J. Supercond. Nov. Magn. **22**, 325 (2009).
[5] M. Angst *et al.*, Phys. Rev. Lett. **88**, 167004 (2002).
[6] J. D. Fletcher *et al.*, Phys. Rev. Lett. **95**, 097005 (2005).
[7] M. Angst *et al.*, Phys. Rev. B **70**, 224513 (2004).
[8] S. Weyeneth *et al.*, arXiv:cond-mat/0911.5420v1 (2009).
[9] M. Eisterer *et al.*, Phys. Rev. B **72**, 134525, (2005).
[10] R. Khasanov *et al.*, Phys. Rev. Lett. **98**, 057007 (2007).
[11] A. Bussmann-Holder *et al.*, J. Supercond. Nov. Magn. **23**, 365 (2010).

11.2 Pressure induced static magnetic order in superconducting $FeSe_{1-x}$

Besides materials containing iron-arsenic layers (*e.g.* FeAs-layers), superconductivity was observed as well in other iron-based compounds as in the $FeSe_{1-x}$ system (1). The transition temperature T_c of $FeSe_{1-x}$ reaches values up to 37 K by applying hydrostatic pressure (2). It has the simplest crystallographic structure among the Fe-based superconductors consisting of layers with a square Fe sheet tetrahedrally coordinated by Se (1). We report on a detailed investigation of the electronic phase diagram of the $FeSe_{1-x}$ system as a function of pressure up to 1.4 GPa by means of AC magnetization and muon-spin rotation measurements. These techniques are direct and bulk sensitive. At a pressure $p \simeq 0.8$ GPa the non-magnetic and superconducting $FeSe_{1-x}$ enters a region where static magnetic order is realized above T_c, and bulk superconductivity coexists and competes on short length scales with the magnetic order below T_c. For even higher pressures an enhancement of both the magnetic and the superconducting transition temperatures, as well as of the corresponding order parameters is observed. These exceptional properties make $FeSe_{1-x}$ to be one of the most interesting superconducting systems investigated extensively at present.

The phase diagram of the recently discovered Fe-based high-temperature superconductors (HTS) shares a common feature with cuprates and heavy fermion systems: The parent compounds of the Fe-based HTS, such as REOFeAs, AFe$_2$As$_2$ (A = alkaline earth metal) and FeCh (Ch = chalcogen) (3; 4; 5) exhibit long-range static magnetic order. Upon doping or application of pressure (chemical or external), magnetism is suppressed and superconductivity emerges.

It is possible to determine T_c as well as the Néel temperature T_N in a region where both magnetism and superconductivity coexist.

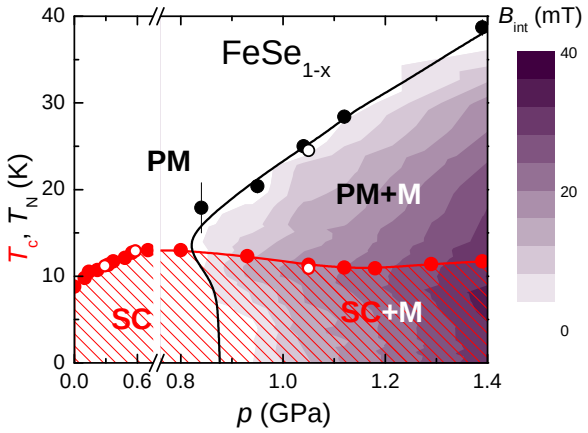

Figure 11.3:
Pressure dependence of the superconducting transition temperature T_c, the magnetic ordering temperature T_N, and the internal field B_{int} (magnetic order parameter) obtained from AC susceptibility and muon-spin rotation experiments of $FeSe_{1-x}$. The $T_c(p)$ and $T_N(p)$ lines are guides to the eye. The closed and the open symbols refer to the samples $FeSe_{0.94}$ and $FeSe_{0.98}$, respectively. SC, M, and PM denote the superconducting, magnetic, and non-magnetic (paramagnetic) states of the sample.

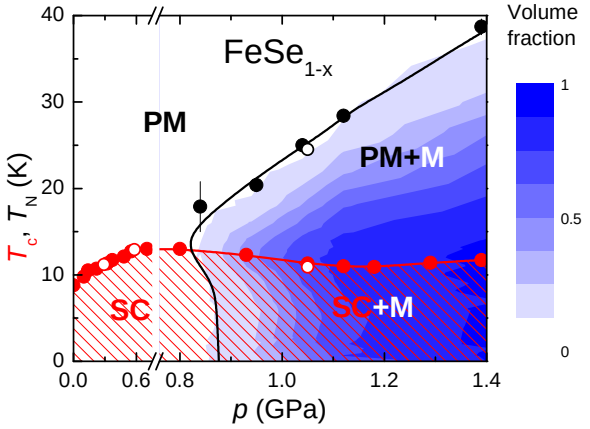

Figure 11.4: Pressure dependence of T_N, T_c, and the magnetic volume fraction of $FeSe_{1-x}$. The meaning of the symbols are the same as in Fig. 11.3.

The here obtained phase diagram is presented in Figs. 11.3 and 11.4. The transition temperature T_c shows a monotonic increase with pressure up to $p \simeq 0.8$ GPa. Static magnetic order is established for $T_c < T < T_N$, and bulk superconductivity sets in below T_c. The competition of the two ground states in this pressure range is evident from the following two observations: First, T_c decreases as a function of pressure as soon as magnetic order appears, leading to the local maximum at $p \simeq 0.8$ GPa in $T_c(p)$ (Fig. 11.5a). Second, the internal field B_{int} (magnetic order parameter), as well as the magnetic volume fraction, decrease as a function of temperature below T_c showing that magnetism, which develops at higher temperatures, becomes partially (or even fully) suppressed by superconductivity (Fig. 11.5b). The superconducting volume fraction is close to 100% for all pressures, while the magnetic fraction increases with increasing pressure and reaches $\simeq$ 90% at the highest pressure $p \simeq 1.39$ GPa. In other words, both ground states coexist in the full sample volume at 1.39 GPa. The data do not provide any indication for macroscopic phase separation into superconducting and magnetic clusters (larger than a few nm in size). Actually, the data rather point to a coexistence of both order parameters on an atomic scale and seem to be stabilized by pressure, since T_c as well as T_N and the magnetic order parameter simultaneously increase with increasing pressure. This observation provides a new challenge for theories describing the mechanism of high-temperature superconductivity (6).

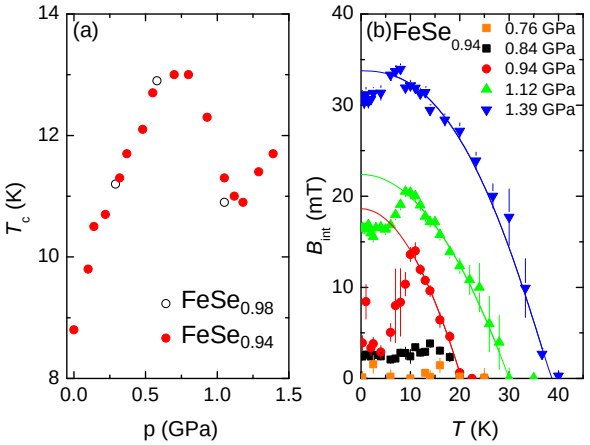

Figure 11.5: (a) Dependence of T_c on pressure p of $FeSe_{0.94}$ and $FeSe_{0.98}$. (b) Dependence of the internal field at the muon stopping site B_{int} which is proportional to the magnetic order parameter. The solid lines represent calculated $B_{int}(T)$ using $B_{int}(T) = B_{int}(0)[1-(T/T_N)^\alpha]^\beta$ in the region $T_c(p) \leq T \leq T_N$ (α and β are the power exponents).

[1] F.-C. Hsu et al., Proc. Nat. Acad. Sci. USA **105**, 14262 (2008).

[2] S. Margadonna et al., Phys. Rev. B **80**, 064506 (2009).

[3] H. Luetkens *et al.*, Nature Mater. **8**, 305 (2009).

[4] A. Jesche *et al.*, Phys. Rev. B **78**, 180504(R) (2008).

[5] R. Khasanov *et al.*, Phys. Rev. B **80**, 140511(R) (2009).

[6] M. Bendele *et al.*, Phys. Rev. Lett. **104**, 087003 (2010).

11.3 NMR investigations of orbital currents in YBCO compounds

The concept of broken symmetry is a possible key element for a comprehensive theory of high-temperature superconductivity. In particular, states with broken time-reversal symmetry have been put forward to explain observations for cuprate high-temperature superconductors (1; 2). The t-J Hamiltonian defines states that break time-reversal symmetry, predicting so-called orbital currents (OCs) that are confined to the CuO_2 planes of the cuprates. Among the most prominent OC patterns are the d-density wave (1) and the circulating current (2) schemes.

The body of experimental evidence is not large but nevertheless contradictory. On the one hand, results from neutron spectroscopy (3) and angle resolved photoemission (4) indicate signatures of OCs, whereas measurements of muon-spin rotation and nuclear magnetic resonance (NMR) fail to provide any trace of the currents (5).

NMR is a suitable method to search for OCs (6), since the magnetic fields inevitably produced by OCs may be directly observed. Selected atoms of the sample serve as local magnetic probes, allowing static fields to be detected by the resonance linewidth broadening, and fluctuating fields from the nuclear spin-lattice relaxation measurements.

No evidence for OCs was found in our previous ^{89}Y-NMR study of the cuprate high-temperature superconductor $Y_2Ba_4Cu_7O_{15-\delta}$ (5). Reported here is the subsequent study of a c-axis oriented powder sample of intrinsically underdoped stoichiometric $YBa_2Cu_4O_8$, where we investigated additional local magnetic fields at the Y-site in the pseudogap regime. The ^{89}Y ($\mathrm{I} = 1/2$) isotope is 100% naturally abundant, and insensitive to electric field gradients because of the absence of a quadrupole moment. The well-defined oxygen stoichiometry of $YBa_2Cu_4O_8$ causes the ^{89}Y-NMR line to become exceedingly narrow, thus offering enhanced precision. In addition, compared to (5), more pronounced OC signatures are expected here because of the larger currents following from the lower doping level.

The temperature dependence of the ^{89}Y resonance linewidth were studied at 100 K for two orientations of an external 9 T field: B_0 perpendicular ($B_0 \parallel c$) and parallel ($B_0 \perp c$) to the CuO_2 planes. The line broadening observed corresponds to an additional magnetic field smaller than 0.05 mT, which we take as the upper bound for static OC fields at the Y-site. Since the line broadening was observed for both field directions, it is unlikely to be caused by OCs, making this a rather conservative estimate.

Any dynamic OCs confined to the CuO_2 planes produce magnetic fields, fluctuating either parallel or perpendicular to the crystallographic c-axis. For the spin-lattice relaxation, only magnetic fields that fluctuate perpendicular to the external field are relevant. The field direction depends on the actual OC pattern and is assumed to be independent of the orientation of the applied field. Consequently the ratio of the relaxation times measured for $B_0 \| c$ and $B_0 \perp c$ must change if non-static OCs appear. The investigation of the temperature dependence of the spin-lattice relaxation ratio did not reveal any significant change. Evaluation of the detection limits determined an upper bound of approximately 0.3 mT for any additional fluctuating field amplitude at the Y-site in the temperature range from 300 K to 100 K.

In conclusion, our ^{89}Y-NMR measurements in the pseudogap phase in $YBa_2Cu_4O_8$ show that any additional static magnetic field at the Y-site must be $\lesssim 0.05$ mT. For fluctuating fields an upper bound for the amplitude of approximately 0.3 mT was determined. These new results significantly tighten the previously established constraints for theories of OCs.

[1] S. Chakravarty *et al.*, Phys. Rev. B **63**, 094503 (2001).
[2] C.M. Varma, Phys. Rev. B **73**, 155113 (2006).
[3] Y. Li *et al.*, Nature **455**, 372 (2008).
[4] A. Kaminski *et al.*, Nature **416**, 610 (2002).
[5] S. Strässle *et al.*, Phys. Rev. Lett. **101**, 237001 (2008).
[6] J. E. Sonier*et al.*, Phys. Rev. Lett. **103**, 167002 (2009).

11.4 Oxygen isotope effects within the phase diagram of cuprates

The role of lattice effects in cuprate HTS still is a heavily debated issue. Over past years, a systematic isotope-effect (OIE) study on T_c and other quantities in cuprate HTS has tried to clarify, which role lattice effects play in cuprate systems (see Ref. (1) and references therein). The observed unusual OIEs are beyond the scheme of conventional BCS theory and strongly suggest that lattice effects are essential in the basic physics of cuprate HTS.

Cuprate HTSs exhibit a rich phase diagram consisting of various phases: long range 3D antiferromagnetic (AFM) order, spin-glass (SG) plus coexisting SG+SC state, superconducting (SC) phase and the so-called pseudogap phase. Recently, we performed a detailed OIE study of the various phases observed in all cuprate superconductors, using $Y_{1-x}Pr_xBa_2Cu_3O_{7-\delta}$ as a prototype system of cuprates (2). The various OIE's observed clearly show that lattice effects are effective in all phases of HTS, imposing serious constraints on theoretical models. So far, only a few OIE studies of the pseudogap state were performed for cuprate HTS close to optimal doping. For example, NMR/NQR studies of $YBa_2Cu_4O_8$ revealed a small OIE on the pseudogap temperature, comparable to the one on T_c (3). This is in contrast to results of inelastic neutron scattering experiments on slightly underdoped $HoBa_2Cu_4O_8$ (4), which revealed a large OIE that is sign reversed with respect to the small OIE on T_c.

In order to complete the OIE study of the various phases in the cuprate system $Y_{1-x}Pr_xBa_2Cu_3O_{7-\delta}$, we investigated the OIE on the pseudogap value in this system as a function of Pr doping by means of NMR experiments. The goal of this study was to get better insight in the nature of the pseudogap phase and in the role of lattice effects to form this phase.

A prominent feature of the pseudogap phenomenon is the characteristic temperature dependence of the relative magnetic shift tensor K in the normal conducting phase of underdoped cuprate superconductors. It is best observed in NMR experiments performed on the Cu nuclei in the CuO_2 plane with the external magnetic field applied parallel to the plane, i.e. the component K_{ab} is determined. For this purpose the two investigated partially (90%) $^{16}O/^{18}O$ exchanged powder samples, $Y_{0.7}Pr_{0.3}Ba_2Cu_3O_{7-\delta}$ and $Y_{0.6}Pr_{0.4}Ba_2Cu_3O_{7-\delta}$, were c-axis aligned.

A fit of the well accepted empirical expression $^{16/18}K = C + b \cdot [1 - \tanh^2(\frac{^{16/18}\Delta}{2T})]$ to the observed temperature dependences of $^{16,18}K_{ab}$ (see Fig. 11.6) yields the values for the pseu-

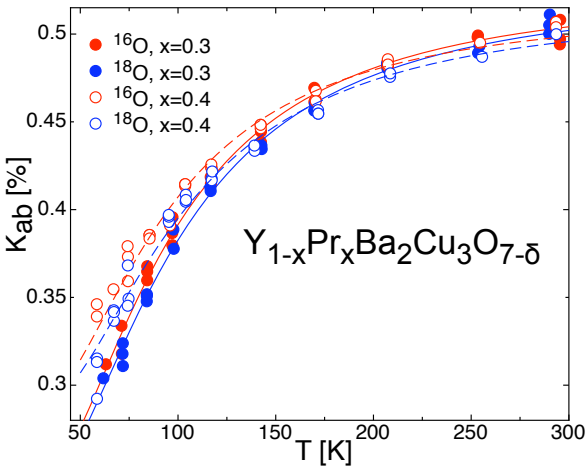

Figure 11.6: Temperature dependence of the magnetic shift K_{ab} of plane ^{63}Cu in $Y_{1-x}Pr_xBa_2Cu_3O_{7-\delta}$ with Pr substitution $x = 0.3$ and $x = 0.4$. Solid and dashed lines are fits to the empirical expression mentioned in the text.

dogap: $^{16}\Delta = 166(6)$ K, $^{18}\Delta = 175(7)$ K for $x = 0.3$ and $^{16}\Delta = 168(7)$ K, $^{18}\Delta = 182(8)$ K for $x = 0.4$, respectively. Using the usual definition we obtain for the OIE coefficient of the pseudo-energy gap value: $\alpha_{0.3}^{\mathrm{PG}} = -0.48(50)$ and $\alpha_{0.4}^{\mathrm{PG}} = -0.74(60)$.

Due to a strongly inhomogeneous distribution of Pr substitution in our samples the observed ^{63}Cu NMR lines are excessively broadened. This leads to insufficient accuracy in determining the lines' frequency positions and the deduced magnetic shifts. Hence, the errors of our results are large and do not allow for a conclusive comparison with other experiments.

[1] H. Keller, in *Superconductivity in Complex Systems*, eds. K.A. Müller and A. Bussmann-Holder, Structure and Bonding **114**, (Springer-Verlag, Berlin, Heidelberg, New York 2005) pp. 114-143.

[2] R. Khasanov *et al.*, Phys. Rev. Lett. **101**, 077001 (2008).

[3] F. Raffa *et al.*, Phys. Rev. Lett. **81**, 5912 (1998).

[4] D. Rubio Temprano *et al.*, Phys. Rev. Lett. **84**, 1990 (2000).